ARTICLES
PUBLISHED ONLINE: 29 JULY 2012 | DOI: 10.1038/NGEO1526
nature geoscience

Massive ice avalanches on Iapetus mobilized by friction reduction during flash heating

Kelsi N. Singer[1]*, William B. McKinnon[1], Paul M. Schenk[2] and Jeffery M. Moore[3]

Long-runout landslides are debris flows or avalanches that travel much farther than expected. They apparently exhibit friction coefficients much lower than either the static or sliding values that are generally accepted for geologic materials. Many friction-reduction mechanisms have been proposed for such landslides observed on Earth and Mars. Here we analyse images from the Cassini mission and report numerous long-runout landslides on Iapetus, an icy satellite of exceptional topographic relief. Its extremely cold, airless surface provides an excellent laboratory for studying long-runout landslides, as influence by trapped atmosphere or groundwater—two proposed friction-reduction mechanisms—is negligible. We use the ratio of drop height to runout length as an approximation for the friction coefficient of landslide material. We find that on Iapetus this ratio falls between 0.1 and 0.3, but does not decrease with increasing length as seen on Earth and Mars. We show that this lack of dependence is consistent with localized frictional heating in ice rubble such that sliding surfaces are slippery. Friction along tectonic faults on icy bodies may be similarly reduced.

Mass movements in the form of landslides or avalanches on some scale are nearly ubiquitous in the Solar System, but large mass movements, in the form of long-runout landslides (or sturzstroms), are far less common[1,2]. Observations of long-runout landslides, principally on Earth[1] and Mars[3–6], have led to a variety of proposed mechanisms for effective friction reduction: riding a cushion of trapped air[7,8]; lubrication by released groundwater, wet debris, or mud[3,4,9]; aqueous pore-pressure support[10,11]; sliding on ice[12] or frictionally generated basal melt layers[13–15]; sliding on evaporitic salt[12]; lubrication by rock flour (nanoparticles)[1,16]; mechanical fluidization[17,18]; fluidization by acoustic waves[19–21]; and even a dependence of the friction coefficient on local gravity[22]. No agreement exists on the fluidization/friction-reduction mechanism necessary for the extraordinary mobility of long-runout landslides and indeed some have questioned whether a friction-reduction mechanism is even necessary[17,23–25]. We find (as in ref. 5) that planetary comparisons under different conditions of gravity, fluid abundance, atmospheric pressure and rock composition can provide key clues to the mechanism(s) of long-runout landslides.

Iapetus is unique among Solar System objects. Although its size (mean diameter 1,470 km) and ice-rich nature (density 1.09 g cm^{-3}) are not remarkable for a mid-size satellite of Saturn, Iapetus has the shape of a body spinning with a period of ∼16 hours (ref. 26), yet at present rotates synchronously with a period of 79.3 days. Iapetus's global albedo pattern is striking, with a strong dichotomy between its dark leading hemisphere and bright trailing hemisphere (with respect to its direction of orbital motion). The body is exceptionally topographically rugged[26–28], with impact-basin depths that exceed 25 km (ref. 28). Iapetus is also the only moon known to have a mountainous equatorial ridge, which reaches heights of ∼20 km at its tallest[26–28] and extends over 75% of the moon's circumference[29]. We show here that Iapetus is also unusual in terms of the number and runout lengths of large landslides. These landslides naturally provide information about the degradation processes and mechanical properties of Iapetus's surface, but more importantly, quantitatively expand the data set on long-runout landslides in the Solar System to the icy satellites. This leads to a testable hypothesis for the mobility of long-runout landslides on icy bodies, with broader implications for ice tectonics and avalanche mobility in general.

Identification and measurement of landslides on Iapetus

Three morphological indicators aided our identification of landslides on Iapetus: first, association with alcoves in an adjacent crater wall or structural ridge; second, distinct surface texture (either hummocky or relatively smooth and uncratered, compared with surrounding terrain); and third, distinct frontal and lateral landslide margins. Landslides were classified into two morphologic types: blocky and lobate; prominent avalanche scars were also noted (Figs 1–3). Thirty mass-movement features were positively identified: 17 of these 30 (both blocky and lobate) are associated with crater rims (termed intracrater) and the remaining 13 are associated with the equatorial ridge (both lobate slides and avalanche scars). Intracrater landslides are found in craters that range in diameter from ∼500 km down to ∼17 km. An additional 18 potential landslides were also identified (Supplementary Tables S1 and S2).

Regional concentrations of landslides (Supplementary Fig. S1) are primarily the result of higher resolution image coverage and favourable viewing geometries in these areas, although the presence or absence of strong topographic variation is also an important factor (that is, the topographically highest section of the equatorial ridge coincides with one concentration of landslides). Approximately equal numbers of intracrater landslides are observed in bright and dark terrain (Supplementary Information) and it should be noted that the difference between dark and bright terrain on Iapetus is widely viewed as superficial (the leading hypothesis considers the dark material to be a coating on a fundamentally icy substrate[30]).

Observed landslide lengths range from a resolution-limited 7 km to up to 80 km, with the longest runouts observed at large

[1]Department of Earth and Planetary Sciences and McDonnell Center for the Space Sciences, Washington University in St Louis, 1 Brookings Drive, St Louis, Missouri 63130-4862, USA, [2]Lunar and Planetary Institute, Houston, Texas 77058, USA, [3]NASA Ames Research Center, Moffett Field, California 94035, USA. *e-mail: knsinger@wustl.edu.

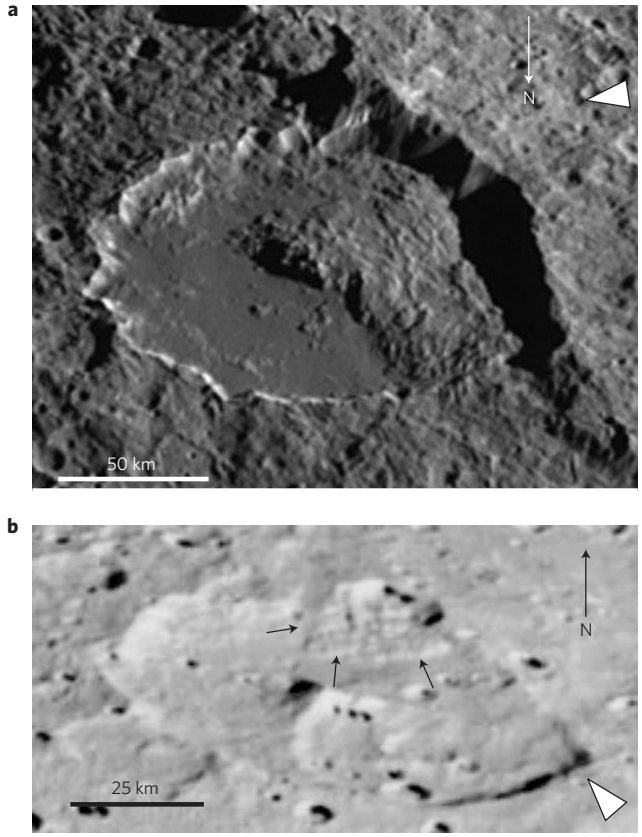

Figure 1 | Example blocky landslides on Iapetus. Blocky landslides are those with a massive, hummocky surface texture (presumably made up of large blocks) and with steep frontal margins. **a**, Type example is the large landslide in Malun crater. This landslide has blocks or textural aspects on the scale of several hundred metres to several kilometres, with an estimated $V \sim 10^5$ km^3 and $H/L \sim 0.12$. **b**, Blocky landslide in the bright material of Charlemagne crater ($H/L \approx 0.11$). Black arrows outline landslide. For Figs 1–3 white arrowheads indicate the approximate illumination direction. Landslide measurements and locations are given in Supplementary Table S2.

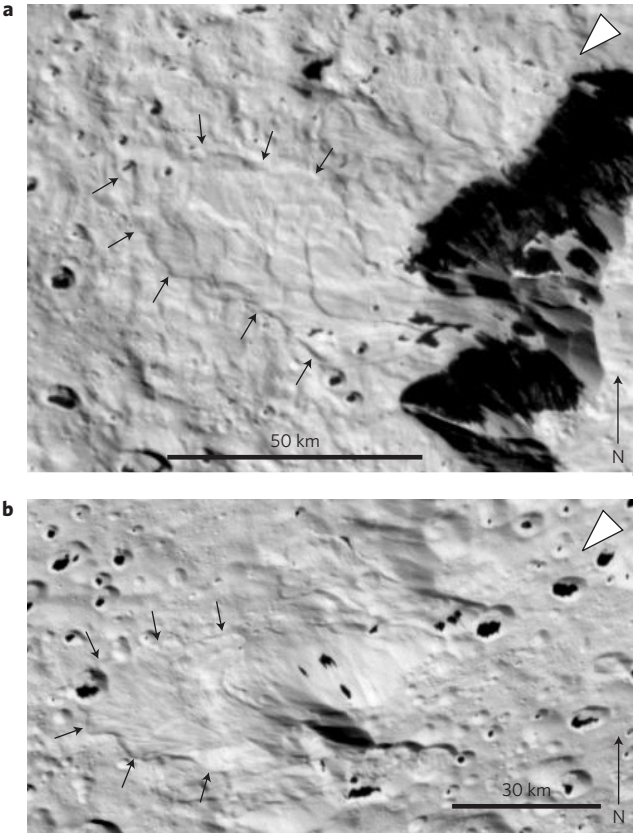

Figure 2 | Example lobate landslides on Iapetus. Lobate landslides have both smoother surface texture (at least at the resolution limit at which they are observed, which is higher in most cases than that of the blocky landslides), indicating they are probably made up of smaller blocks/debris, and lobate margins, which are not as tall and/or steep as in the case of blocky landslides (Fig. 1). **a**, Type example, near the eastern wall of Engelier Basin, has several overlapping lobes and lobate margins ($H/L \approx 0.13$). **b**, Lobate landslide near the eastern wall of Gerin Basin ($H/L \approx 0.15$). Black arrows outline landslides.

impact-basin walls (for example, Engelier, Fig. 2) and the equatorial ridge (Fig. 3). Drop heights were measured from stereo-derived topography (examples in Fig. 4). Values for drop height range from ~1 to 12.5 km, with the tallest scarps being the ridge or large basin walls (Supplementary Table S1). Maximum landslide velocities for these drop heights, assuming free fall conditions, would be ~20–75 m s^{-1} (gravity on Iapetus is 0.224 m s^{-2}). Landslide volumes, as well as aspect ratios (geometries) for the initial collapse masses, can be determined from our stereo topography in a handful of cases (see Methods and Supplementary Fig. S4).

Comparison with landslides on other planetary bodies

Landslides on Iapetus are the largest and most numerous observed on any icy body, and rival the longest (and most voluminous) runout landslides seen elsewhere in the Solar System (for example, those associated with the steep canyon walls of the Valles Marineris system on Mars[3–6] or with Euboea Montes on Io[31]). With respect to icy worlds, mass movements of relatively modest scale (more akin to debris aprons) have been detected on Jupiter's moon Callisto[32], instances are known on Saturn's small moon Phoebe[27] and we here identify two on Saturn's moon Rhea (Supplementary Information).

The ratio of runout length to drop height (L/H) gives a measure of the efficiency or mobility of an avalanche; its inverse (H/L) is an approximation to the coefficient of friction of the sliding debris and is useful as a comparative measure (for example, refs 2,5,21 and see Supplementary Information). In Fig. 5 we plot H/L for our Iapetus avalanches (both blocky and lobate) as a function of runout length (a proxy for volume), along with values from other Solar System bodies for comparison. The offset trends of decreasing H/L with increasing landslide length (or volume) for rock avalanches on the Earth and landslides on Mars have been known for some time[5,6,11,21]. Notably, the H/L for Iapetus landslides do not trend downwards with increasing L, but scatter in the range of 0.1–0.3 regardless of length. This is consistent with frictional control on runout length, but unlike the terrestrial and martian trends (see linear fits), does not indicate a role for a gravity-independent yield strength, such as predicted by Bingham or acoustic fluidization models[5,11].

The range of H/L for Iapetus landslides is, moreover, bounded. Values in excess of 0.3, typical for small terrestrial rock avalanches and martian landslides[1,6,21], are not seen; neither are exceptionally low values of $H/L \ll 0.1$, typical of terrestrial submarine landslides and mudflows (for example, ref. 33). Similar ranges in H/L are seen when lobate or blocky landslides on Iapetus are considered separately (Fig. 5). Furthermore, the effective landslide friction coefficient is not different at different locations on Iapetus (Supplementary Fig. S2): landslides on the equatorial ridge have the same average H/L as intracrater landslides. When either lobate or blocky landslides are considered alone, however, there is some indication of decreasing H/L with L. The trends are not strong,

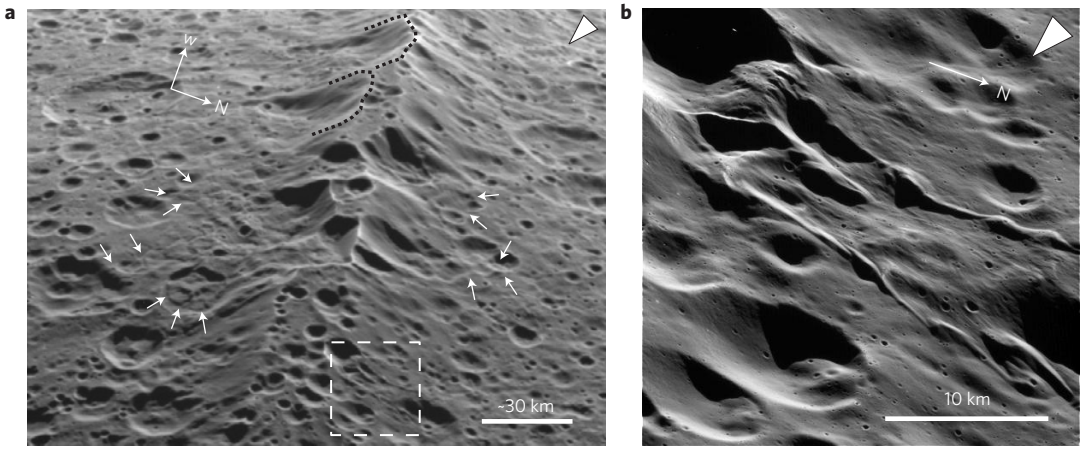

Figure 3 | Landslide modification of Iapetus's equatorial ridge. a, Section of the equatorial ridge illustrating both lobate landslides with sharp-walled alcoves (arrows outline the toe of deposits, with $V \sim 10^4$ km^3 and $H/L \approx 0.13$ for slide at lower left). More degraded avalanche scars (dotted outlines) are alcoves with no visible landslide flows, presumably the sites of ancient landslides. There is widespread modification of the ridge through mass wasting. **b**, Inset from white dashed square in **a**, and one of the highest resolution images (48 m per pixel) of an Iapetus landslide, showing a lobate landslide with raised lateral margins or levees.

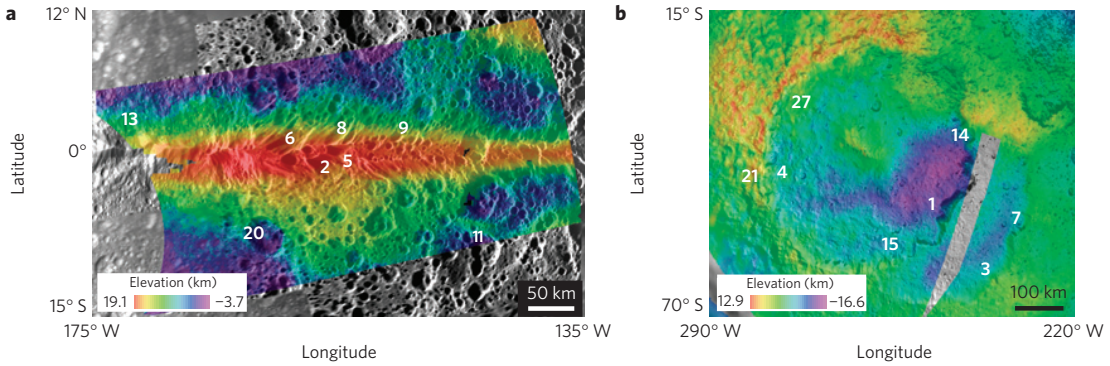

Figure 4 | Stereo-derived DEMs of Iapetus's surface. a, Portion of Iapetus's equatorial ridge and **b**, Engelier Basin, overlaid on simple cylindrical and orthographic image bases, respectively. The ridge image base exhibits layover (parallax distortion) owing to the extreme viewing angle of the original images. Both ridge and basin rim exhibit large lobate landslides (numbered; see Supplementary Table S2).

though; weighted least-squares fits of H/L versus log L yield slopes of -0.38 ± 0.22 and -0.21 ± 0.10 for lobate and blocky landslides, respectively, which are consistent with zero slope at the 2σ level.

We conclude that whereas friction must be an important governing rheological parameter for landslides on Iapetus, the effective coefficients of friction implied are significantly less than those generally thought applicable to static or sliding friction of dry rock (for example, Byerlee's rule)[34]. More to the point, the effective coefficients of friction are much less than that measured for very cold (77–115 K) water ice in the laboratory (0.55–0.7 at the overburden pressures characteristic of Iapetus landslides, <5 MPa; ref. 35). Also, for those few landslides where we can determine the initial aspect ratios of the collapse mass (see Methods), the normalized runouts are large (comparable to or greater than those of martian landslides), which further suggests a friction-reduction or mobilization mechanism (Supplementary Fig. S5).

Landslide mechanics and implications for ice friction

Iapetian landslides have low-to-modest effective coefficients of friction. On Earth and Mars, similar values are often thought to imply basal pore-pressure support by water or trapped gas[11]. Subsurface temperatures on Iapetus, time averaged, are quite low, less than 100 K on the dark hemisphere and less than 75 K on the bright[36], so the influence of liquid water or water vapour seems dubious (although we consider CO_2 in the Supplementary Information). Ice friction is a function of temperature and sliding velocity, however, and for sufficient sliding velocities (easily met by the landslides here) and temperatures warmer than −30 °C or so, the friction coefficient for ice can be 0.1 or less (as commonly experienced, ice is slippery)[37,38]. We suggest that frictional dissipation along cold sliding ice surfaces within and near the base of landslides on Iapetus may have raised temperatures on these surfaces into the slippery regime and permitted the relatively long runouts observed. Such a mechanism is obviously not directly applicable to terrestrial sturzstroms, but it is related in principle to hypotheses of landslide lubrication by basal melt layers (psuedotachylite or frictionite)[13–15] and the energetics are favourable (see below). Most notably, if true, it implies a commensurate reduction in friction along faults within icy crusts, in a manner similar to that proposed for faults in rock[39,40].

Whether low ice friction is the single most important rheological parameter governing landslide motion on Iapetus or whether a Bingham (viscoplastic) or acoustic fluidization rheology is also compatible should be tested through numerical landslide modelling (for example, ref. 11). The H/L values for ice avalanches on Iapetus (Fig. 5) do imply some mechanism to lower the internal friction of the sliding mass. Acoustic fluidization is a possibility, but as noted, the lack of a distinct overall H/L versus L trend does not require it (that is, to assume acoustic fluidization would be *ad hoc*[11]). In this regard, from a scaling or dynamic similarity point of view,

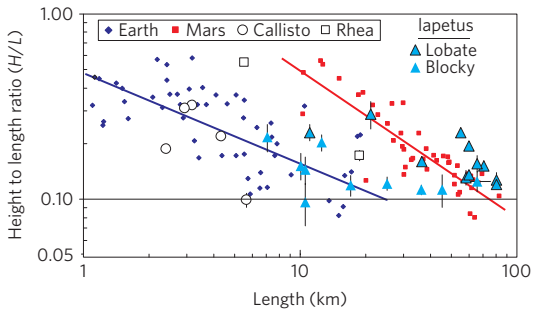

Figure 5 | Iapetus landslide mobilities in comparison. Shown are measurements for: terrestrial subaerial landslides (from ref. 46); martian landslides in Valles Marineris[6], a high-resolution data set that supersedes earlier Viking-based measurements[5]; debris aprons within several craters on Jupiter's moon Callisto (updated from ref. 46); and landslides within two young craters on Rhea, the saturnian moon most comparable to Iapetus (see Supplementary Fig. S3). H/L and L are proxies for the coefficient of friction and volume, respectively. Iapetian landslides exhibit a range of friction values (mobilities) similar to that of Earth and Mars, but do not show the same trend of decreasing H/L with increasing L. Standard stereo errors are indicated.

landslides on Iapetus are equivalent to slides on (icy) Callisto[32] that are reduced in linear dimension by a factor of 6 (so that the product ρgH, or ρgL, where g is gravitational acceleration and ρ is density, remains constant) and equivalent to even smaller landslides on Mars (an additional reduction factor of 7.5, for a total factor of 45, owing to Mars's greater gravity and material density). Thus it may not be so unusual that iapetian landslides do not show decreasing H/L with increasing L over the range of L in Fig. 5; to test for the influence of a non-gravity-dependent yield strength, more observations of landslides of even greater scale on Iapetus might be required, or (more likely to be realized in practice) recognition of sufficiently small landslides of greater H/L (as may be the case for Callisto and possibly Rhea; Fig. 5). In terms of a Bingham rheology, we note that order-of-magnitude estimates of landslide yield strength on Iapetus (where slopes can be constrained) are consistent with dry as opposed to fluid-saturated debris (Supplementary Information).

The simplest explanation for reducing internal friction in large ice avalanches is shear heating along sliding, icy contact surfaces. The characteristic, specific potential energy release during an avalanche is gH, which for $H = 1$–12.5 km on Iapetus (Supplementary Table S1) equates to 0.2–2.8 kJ kg^{-1}. These values can be compared with the ~200 kJ kg^{-1} required to bring water ice from 100 K to a slippery 250 K or the 335 kJ kg^{-1} needed to melt it[41]. It is clearly much easier to warm ice until it is slippery than to melt it; moreover, any liquid water would rapidly be expelled from sliding surfaces, because any icy sturzstrom would be dilatant and porous. Hence we favour modest heating over melting as a friction-reduction mechanism. The volume fraction of heated ice would nevertheless be small, 0.1–1.4% of the total for the drop heights above. What these percentages imply is that for friction reduction to be effective, dissipation must be localized along one or more sliding surface, not distributed throughout the body of the icy landslide (see additional discussion in Supplementary Information).

Slippery ice is not an argument for lubrication by frictional melt (water) or pore-pressure support. One mechanism proposed for friction reduction in ice itself is, however, surface premelting[42] (although this phenomenon is actually not obvious or agreed on[38,41]). If premelting does occur, then a small but non-trivial water vapour pressure is implied. The vapour pressure of both ice and supercooled water near −30 °C is just a few tens of pascals[41], which given the internal pressures in large landslides on Iapetus, would seem easy to maintain on sliding surfaces in contact. Fundamentally, our point is that ice possesses a well established property such that, for sufficient sliding velocity and temperature, dynamic friction is quite low[37,38]. Whether such low sliding friction can be demonstrated for initially cold (<100 K) ice in a vacuum has not been experimentally attempted (to our knowledge), but would be an important and direct test of the hypothesis we offer here.

Implications for Iapetus's equatorial ridge and surface

The relative bounty of landslides on Iapetus probably owes to several factors. One would be the spectacular topography found there and another the extreme age of the surface as implied by crater counts[26]. Iapetus has some of the greatest topography relative to its size of any major body in the Solar System, with large impact-basin rims higher than 10 km and the equatorial ridge reaching 20 km in height. Maintenance of such variations and the global non-equilibrium shape imply a thick ice lithosphere and relatively low heat flows, and are consistent with a lack of active tectonics and (cryo)volcanic activity over Iapetus's long history[29]. As such, landslides on Iapetus are most likely to be triggered over time by nearby impacts or by the seismic effects of large, distant impacts. Furthermore, Iapetus's orbital position far from Saturn means relatively low gravitational focusing and a relatively low rate of cometary bombardment, compared with other icy satellites[43]. This has probably permitted the survival of marginally stable slopes over geologic time and markedly reduced the rate of impact degradation of all landforms over time, especially by so-called sesquinary impactors (those generated internal to the Saturn system)[43].

The sculpting of Iapetus's topography by mass wasting, both along the equatorial ridge and the rims of large impact basins, is remarkable. The implication is that the surface and upper crust of the satellite is, along with the factors noted above, largely unconsolidated. This is consistent with dominance of impact cratering, as opposed to other resurfacing processes, over geological history, and the non-volatile nature of the volumetrically dominant crustal mineral (water ice) at the low temperatures and pressures of the subsurface.

The strongly backcut and fluted impact-basin rims on Iapetus are particularly unusual (for example, Fig. 4b), and similar morphologies are generally not seen around large impact craters and basins in the Solar System. In terms of comparably sized structures on other mid-sized icy satellites, the degraded basins on Rhea bear some resemblance, but the relatively young and undegraded Odysseus Basin on Tethys does not. This suggests that an additional factor may be in play on Iapetus. One possibility is a more volatile ice component, such as CO_2 (see Supplementary Information). We note that the most crenulated portions of the Engelier Basin wall are associated with a depression (Fig. 4b), probably related to Engelier forming over an older, large basin (Gerin, Supplementary Fig. S6). Most landslides in Engelier occur in this eastern section (Fig. 2a and Supplementary S1) and may be related to a reduced structural integrity owing to the Gerin impact.

Regarding the equatorial ridge, it shows diverse morphologies where it is visible. The mountainous peaks on the ridge are variable, sometimes sharp and steep, and at other places rounded, flat-topped or exhibiting numerous parallel ridge crests. Landslides and alcoves are most prevalent in the tall, steep sections. Along with cratering, much of this variability and variable preservation along strike can be attributed to mass wasting altering the appearance of the ridge over time (Supplementary Fig. S7). The ridge does not seem to be constructed of particularly coherent material. No matter how the ridge originally formed[44], it has since been considerably altered. Ridge flank slopes are neither pristine, nor in the long term, stable. Arguments against an exogenic origin for the ridge based on slope angles[26] should take these observations into account.

Methods

Landslides were identified in original Cassini mission images, with resolutions as good as 450 m per pixel on Iapetus's bright, trailing hemisphere and as good as 870 m per pixel on its dark, leading hemisphere (from the September 2007 and December 2004 close encounters, respectively). Landslides were then mapped in ArcGIS and runout lengths were measured geodesically. Stereo topography was used to determine landslide drop heights and, in some cases, landslide deposit thicknesses (Supplementary Fig. S4). Sufficient Cassini images exist to construct a global digital elevation model (DEM) covering 80% of Iapetus's surface, using an automated stereo photogrammetry method based on scene-recognition algorithms[31,45]. Spatial resolutions are controlled by the lower resolution image in the stereo pair and, using this method, are further reduced by a factor of three to five. Stereo coverage exists in all areas of interest (that is, where landslides have been positively identified). Vertical precisions were calculated through standard stereo technique from $mr_p(\tan e_1 + \tan e_2)$, where m is the accuracy of pixel matching (0.2–0.3), r_p is pixel resolution and e_1 and e_2 are the emission angles of the stereo image pair, and reach ±150 m over the highest section of the Iapetus ridge.

Drop heights were measured from the head of a given landslide scarp to the top of the toe of the corresponding landslide deposit, which is a best practice using topography alone to approximate the vertical displacement of the centre of mass of a given landslide[2,5]. Heights were determined from topographic profiles along the same line as the length was measured (typically down the centre of the landslide). We also examined profiles to either side of the centre axis of the landslide. In case of variability in the height of the head of the scarp or toe of the deposit, an average of several profiles was used. The stereo DEM is referenced to Iapetus's biaxial figure. Iapetus's global figure is, as noted, non-hydrostatic. Iapetus's dynamic topography owing to its fossil bulge is thus greater by ~14 km equator-to-pole. We do not correct our drop heights to account for this, but note that the largest change would be an increase by 150 m for one (north–south) ridge landslide (number 2); east–west landslides and east–west topography are unaffected.

Volume (V) determinations for landslides on Iapetus are limited to those few sites where the pre-avalanche scar geometry can be reasonably estimated (such as along the flat-topped section of the equatorial ridge; Supplementary Fig. S4b) or where landslide volume can be determined directly from the DEM (that is, Malun crater; Supplementary Fig. S4a). In other cases, such as the eastern wall of Engelier Basin (Fig. 2b), the avalanche scar is clear, but the landslide is composed of numerous overlapping lobes that were apparently emplaced over time; in this case the avalanche scar volume would be a severe overestimate for any single landslide lobe. Initial aspect ratios can also be determined from the same pre-avalanche scar geometry for equatorial ridge slides; for the Malun slide we reconstruct the pre-avalanche geometry assuming the landslide volume extended from the crater floor to the headscarp.

Received 27 January 2012; accepted 20 June 2012; published online 29 July 2012

References

1. Hsü, K. J. Catastrophic debris streams (sturzstroms) generated by rockfalls. *Geol. Soc. Am. Bull.* **86,** 129–140 (1975).
2. De Blasio, F. V. *Introduction to the Physics of Landslides* (Springer, 2011).
3. Lucchitta, B. K. Landslides in Valles Marineris, Mars. *J. Geophys. Res.* **84,** 8097–8113 (1979).
4. Lucchitta, B. K. Valles Marineris, Mars—Wet debris flows and ground ice. *Icarus* **72,** 411–429 (1987).
5. McEwen, A. S. Mobility of large rock avalanches: Evidence from Valles Marineris, Mars. *Geology* **17,** 1111–1114 (1989).
6. Quantin, C., Allemand, P. & Delacourt, C. Morphology and geometry of Valles Marineris landslides. *Planet. Space Sci.* **52,** 1011–1022 (2004).
7. Shreve, R. L. Sherman landslide, Alaska. *Science* **154,** 1639–1643 (1966).
8. Shreve, R. L. The Blackhawk landslide. *Spec. Pap. Geol. Soc. Am.* **108,** 1–47 (1968).
9. Legros, F. The mobility of long-runout landslides. *Eng. Geol.* **63,** 301–331 (2002).
10. Johnson, B. in *Rockslides and Avalanches, 1, Natural Phenomena* (ed. Voight, B.) 481–504 (Elsevier Science, 1978).
11. Harrison, K. P. & Grimm, R. E. Rheological constraints on martian landslides. *Icarus* **163,** 347–362 (2003).
12. De Blasio, F. V. Landslides in Valles Marineris (Mars): A possible role of basal lubrication by sub-surface ice. *Planet. Space Sci.* **59,** 1384–1392 (2011).
13. Erismann, T. H. Mechanisms of large landslides. *Rock Mech.* **12,** 15–46 (1979).
14. De Blasio, F. V. & Elverhøi, A. A model for frictional melt production beneath large rock avalanches. *J. Geophys. Res.* **113,** F02014 (2008).
15. Weidinger, J. T. & Korup, O. Frictionite as evidence for a large Late Quaternary rockslide near Kanchenjunga, Sikkim Himalayas, India—Implications for extreme events in mountain relief destruction. *Geomorphology* **103,** 57–65 (2009).
16. Han, R., Hirose, T., Shimamoto, T., Lee, Y. & Ando, J. Granular nanoparticles lubricate faults during seismic slip. *Geology* **39,** 599–602 (2011).
17. Davis, T. R. H. Spreading of rock avalanche debris by mechanical fluidization. *Rock Mech. Rock Eng.* **15,** 9–24 (1982).
18. Campbell, C. S., Cleary, P. W. & Hopkins, M. J. Large-scale landslide simulations: Global deformation, velocities and basal friction. *J. Geophys. Res.* **100,** 8267–8283 (1995).
19. Melosh, H. J. Acoustic fluidization—A new geologic process? *J. Geophys. Res.* **84,** 7513–7520 (1979).
20. Melosh, H. J. The physics of very large landslides. *Acta Mech.* **64,** 89–99 (1986).
21. Collins, G. S. & Melosh, H. J. Acoustic fluidization and the extraordinary mobility of sturzstroms. *J. Geophys. Res.* **108,** 2473–2486 (2003).
22. Kleinhans, M. G., Markies, H., de Vet, S. J., in't Veld, A. C. & Postema, F. N. Static and dynamic angles of repose in loose granular materials under reduced gravity. *J. Geophys. Res.* **116,** E11004 (2011).
23. Lajeunesse, E. *et al.* New insights on the runout of large landslides in the Valles-Marineris Canyons, Mars. *Geophys. Res. Lett.* **33,** L04403 (2006).
24. Staron, L. & Lajeunesse, E. Understanding how the volume affects the mobility of dry debris flows. *Geophys. Res. Lett.* **36,** L12402 (2009).
25. Holsapple, K. A. On the flow and fluidization of granular materials: Applications to large lunar craters, cliff collapses, and asteroid shapes. *42nd Lunar Planet. Sci. Conf.* abs. #2612 (2011).
26. Giese, B. *et al.* The topography of Iapetus' leading side. *Icarus* **193,** 359–371 (2008).
27. Porco, C. C. *et al.* Cassini imaging science: Initial results on Phoebe and Iapetus. *Science* **307,** 1237–1242 (2005).
28. Schenk, P. M. *AAS/Division for Planetary Sciences Meeting 42* abs. #9.16 (2010).
29. Singer, K. N. & McKinnon, W. B. Tectonics on Iapetus: Despinning, respinning, or something completely different? *Icarus* **216,** 198–211 (2011).
30. Spencer, J. R. & Denk, T. Formation of Iapetus' extreme albedo dichotomy by exogenically triggered thermal ice migration. *Science* **327,** 432–435 (2010).
31. Schenk, P. M. & Bulmer, M. H. Origin of mountains on Io by thrust faulting and large-scale mass movements. *Science* **279,** 1514–1517 (1998).
32. Chuang, F. C. & Greeley, R. Large mass movements on Callisto. *J. Geophys. Res.* **105,** 20227–20244 (2000).
33. Hampton, M. A. & Locat, J. Submarine landslides. *Rev. Geophys.* **34,** 33–59 (1996).
34. Jaeger, J. C., Cook, N. G. W. & Zimmerman, R. W. *Fundamentals of Rock Mechanics* Ch. 3 (Wiley–Blackwell, 2007).
35. Beeman, M., Durham, W. B. & Kirby, S. H. Friction of ice. *J. Geophys. Res.* **93,** 7625–7633 (1988).
36. Kimura, J. *et al.* Sublimation's impact on temporal change of albedo dichotomy on Iapetus. *Icarus* **214,** 596–605 (2011).
37. Maeno, N. & Arakawa, M. Adhesion shear theory of ice friction at low sliding velocities, combined with ice sintering. *J. Appl. Phys.* **95,** 134–139 (2004).
38. Kietzig, A-M., Hatzikiriakos, S. G. & Englezos, P. Physics of ice friction. *J. Appl. Phys.* **107,** 081101 (2010).
39. Di Toro, G. *et al.* Fault lubrication during earthquakes. *Nature* **471,** 494–498 (2011).
40. Goldsby, D. L. & Tullis, T. E. Flash heating leads to low frictional strength of crustal rocks at earthquake slip rates. *Science* **334,** 216–218 (2011).
41. Petrenko, V. F. & Whitworth, R. W. *Physics of Ice* (Oxford Univ. Press, 1999).
42. Rosenberg, R. Why is ice slippery? *Phys. Today* **58,** 50–55 (2005).
43. Dones, L. *et al.* in *Saturn from Cassini-Huygens* (eds Dougherty, M. K., Esposito, L. W. & Krimigis, S. M.) 613–635 (Springer, 2009).
44. Dombard, A. J., Cheng, A. F., McKinnon, W. B. & Kay, J. P. Delayed formation of the equatorial ridge on Iapetus from a sub-satellite created in a giant impact. *J. Geophys. Res.* **117,** 03002 (2012).
45. Schenk, P. M., Wilson, R. R. & Davies, A. G. Shield volcano topography and the rheology of lava flows on Io. *Icarus* **169,** 98–110 (2004).
46. Moore, J. M. *et al.* Mass movement and landform degradation on the icy Galilean satellites: Results of the Galileo nominal mission. *Icarus* **140,** 294–312 (1999).

Acknowledgements

This work was supported by grants from the NASA Planetary Geology and Geophysics Program (W.B.M.) and Cassini Data Analysis Program (J.M.M. and P.M.S.) and by a NESS Fellowship to K.N.S. We sincerely thank A. Lucas for comments that substantially improved this paper, and dedicate this work to the memory of R. Greeley.

Author contributions

K.N.S. collected the landslide data and along with W.B.M. compiled the literature data and wrote the paper. P.M.S. created and supplied the topography data used here and along with J.M.M. contributed to discussion of the data and revisions to the manuscript.

Additional information

Supplementary information is available in the online version of the paper. Reprints and permissions information is available online at www.nature.com/reprints. Correspondence and requests for materials should be addressed to K.N.S.

Competing financial interests

The authors declare no competing financial interests.